

Iterated Unscented Kalman Filter-Based Maximum Power Point Tracking for Photovoltaic Applications

A. K. Abdelsalam

Electrical Engineering Department
Arab Academy for Science and Technology &
Maritime Transport
Alexandria, (Egypt)

Shu Goh, O. Abdelkhalik

Department of Mechanical
Engineering
Michigan Technological
University, (USA)

S. Ahmed

Electrical and computer
Engineering Department
Texas A&M University at
Qatar, (Qatar)

A. Massoud

Electrical Engineering
Department
Qatar University,
(Qatar)

Abstract— One of main challenges in harvesting power from a PV source is maximum power point tracking (MPPT). This is due to the nonlinear behaviour and characteristics of PV arrays. Conventional MPPT techniques usually utilize a hill climbing process which requires partial/full scan of the array power-voltage (P-V) curve resulting in high power fluctuation during peak searching. Dynamic estimation techniques, such as the Kalman filter, benefit from their ability to estimate non-measurable signals with rapid convergence. In this paper, a MPPT technique based on the Iterated Unscented Kalman Filter (IUKF) is presented. The proposed technique achieves: (i) satisfactory MPPT for PV arrays working under varying environmental conditions, (ii) PV array modelling with full parameter estimation including temperature and insolation level, and (iii) full estimation of the working P-V curve for the PV array. Only six measurement points are required for MPPT, modelling, and curve estimation; hence no full scan for the P-V curve is needed. This paper presents the system mathematical model and simulations. Moreover, an experimental setup is implemented illustrating practical results at various insolation levels and temperatures to validate the proposed technique.

Keywords— Photovoltaic, Maximum Power Point, Maximum Power Point Tracking, Kalman Filter.

I. INTRODUCTION

Renewable energy sources depend on many performance metrics such as efficiency, reliability, cost, grid connection regulations, energy storage cost, and advanced control algorithm implementation [1-2]. Among the varying sources of renewable energy, the most common are hydropower, wind, and photovoltaic (PV) [1]. Examining PV characteristics reveals the fact that the available power from any PV array varies nonlinearly with the solar insolation.

This variation, in addition to the dependency on the array temperature, creates the intermittent nonlinear PV power behavior. Hence, the available power from any PV source needs to be tracked as it varies with the environmental conditions. Therefore, adequate maximum power point tracking (MPPT) is unavoidable [3]. Numerous MPPT techniques have been proposed for PV optimum operating point tracking [3].

These techniques vary in complexity, requirements, convergence speed, cost, effectiveness, and implementation. Hill climbing [4-7] and perturb and observe (P&O) [8-11] methods are the most common MPPT techniques. In these techniques, the tracking process is repeated periodically until the MPP is located. The system then oscillates about this MPP. The oscillation can be minimized by decreasing the perturb value. However, a smaller perturb slows down the system. A variable-perturb-value approach that decreases the perturb value towards the MPP is an alternative. The incremental conductance (IncCond) [12-15] technique relies on the fact that the slope of the PV array power curve is zero at the MPP. Fast tracking is possible with bigger increments but the system might not operate exactly at the MPP and instead oscillate about it; exhibiting a similar trade off as that of the P&O technique. Another technique utilizes the linear relation between the voltage at the maximum power point and the array open circuit voltage at different environmental conditions [16-18]. Once the relation is known, the voltage at the maximum power can be computed using the array open circuit voltage measured periodically by momentarily shutting down the power converter. Some disadvantages exist, mainly temporary power loss. To prevent this power loss, pilot cells from which the array open circuit voltage can be obtained without shutting down the power converter are used [16], but this is usually accompanied by additional cost and wiring complexity [3]. Utilizing the fact that the current at the maximum power point has a nearly linear relation with the PV array short circuit current, other tracking techniques are reported [16, 17, 19]. However, measuring the PV array short circuit current during operation is a critical problem, as an extra switch has to be added to the power converter to periodically short circuit the PV array. This increases the system cost and the number of components. Fuzzy logic controllers are able to work with imprecise inputs, mathematical model independency, and system nonlinearity tolerance. A seven fuzzy level method is used as MPPT technique in [20-21]. MPPT fuzzy logic controllers perform well under varying environmental conditions. However, their effectiveness suffers from designer dependency in selecting the proper error computation and the rule base table [3]. Artificial intelligence, especially neural

networks, can be used for MPPT [22-24].

The Kalman filter (KF), as a dynamic estimation technique, has played an important role in many industrial applications as speed sensorless estimation in electric drives [25-27], non-linear mechanical loads [28], power system protection and harmonics estimation [29-30], robots/particles localization [31-33], and fault diagnostics [34]. Also, KF-based techniques are widely used in distributed generation and islanding detection applications [35-36]. The ability to estimate non-measurable signals, fast convergence, and direct implementation encourages wider utilization of KF-based techniques in various industrial applications. One classification in estimation problems is linear vs. nonlinear, depending on whether the system model and/or measurements model are linear or nonlinear functions of the states [37-39]. Of the most popular nonlinear estimation algorithms are the Extended KF (EKF), Iterated Extended KF, and Iterated Unscented KF (IUKF) [40].

From the previous discussion, it can be seen that the MPPT problem is characterized by the following. First, a dynamic model is available with uncertainty in some of the model parameters. Second, a number of measurement points (power versus voltage) can be collected during operation. Hence, KF is suitable for dynamic estimation of the MPP. EKF is appropriate and fast for real-time processing specially with priori information of the measurement and process noise covariance. The trade-off between the computational burden and error introduced by neglecting the high order terms in linearization is a bottleneck. This can be overcome by employing IUKF. In this paper, an IUKF-based algorithm for PV MPPT application is proposed. The presented technique is capable of determining the operating point for the maximum available power without any hill climbing process. It utilizes only six operating points on the array P-V curve, in addition to the stored PV array data sheet curves to estimate the actual operating P-V curve then jumps directly to the maximum power operating point without any perturb and observe steps. The proposed technique estimates, as a by-product, the PV array characteristic parameters. The estimated parameters are: ideality factor, reverse saturation current, equivalent series resistance, equivalent parallel resistance, array temperature, and incident solar insolation.

II. PV CHARACTERISTICS AND MODELLING

In this section, the characteristics of a typical PV array are illustrated showing the need for MPPT. In addition, PV cell modelling is discussed showing the necessary parameters needed for full model description.

A. PV array characteristics

PV arrays are characterized by the non-linear behaviour of voltage and current relations. Typical PV array characteristics are shown in Fig. 1. As shown in Fig. 1, in addition to the nonlinear relation between the PV array voltage and current, the relation is dependent on external environmental conditions, temperature, and insolation. These dependencies and

nonlinearity create a challenge in any PV application. To further illustrate using a practical example, the KYOCERA KC50T PV array [41] is simulated using the MATLAB/SIMULINK package, plotting the variation of its power versus voltage curve at different insolation levels as shown in Fig. 2. It can be shown from Fig. 2 that the maximum power point is variable with insolation, as well as temperature. The array voltage, corresponding to the maximum power point, is not fixed either. Hence, tracking is mandatory to force the PV array to operate at its available maximum power point.

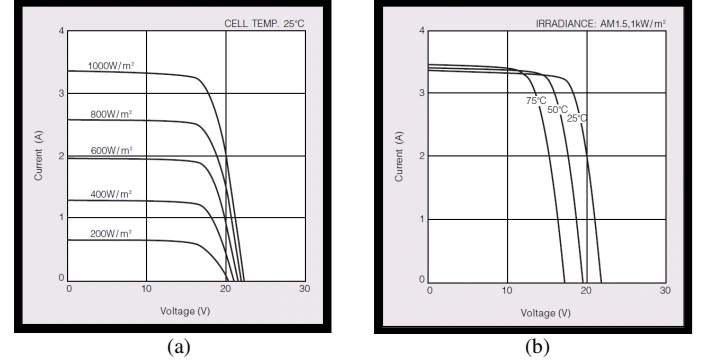


Fig. 1: Typical PV array characteristics, KYOCERA KC50T PV [41]
(a) Variation of PV characteristics with solar irradiance, $T = 25^{\circ}\text{C}$
(b) Variation of PV characteristics with temperature, irradiance = 1000 W/m^2

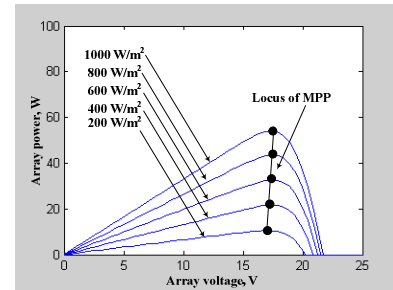


Fig. 2: KYOCERA KC50T PV array [41] simulation for array power variation with array voltage for different insolation levels at constant temperature of 25°C

B. PV cell model

Fig. 3 shows the single-diode equivalent circuit of a PV cell [42]. There is also double-diode model for PV cell [43], but the single-diode model is accurate enough for most MPPT applications so it is used in this paper. The light-generated current, I_l , is proportional to insolation G , and can be written as shown in (1);

$$I_l = \left(\frac{G}{G_0}\right) I_{g0} + J_0(T_c - T_{ref}) \quad (1)$$

where G_0 is the reference insolation, I_{g0} is the current at G_0 , J_0 is the temperature coefficient of I_l , T_c is the absolute temperature of the cell in Kelvin, and T_{ref} is the reference cell temperature in Kelvin. The reference insolation is often taken as $G_0 = 1 \text{ kW/m}^2$. The diode current I_d is given by the Shockley's equation shown in (2);

$$I_d = I_0 \left[\exp \left(\frac{q(V + IR_s)}{nkT_c} \right) - 1 \right] \quad (2)$$

where the quantity $V + IR_s$ is the voltage across the diode, I_0 is the reverse saturation current, q is the electron charge, V and I are the cell voltage and current, R_s is the series resistance, n is the ideality factor, and k is the Boltzmann's constant. The reverse saturation current I_0 is sensitive to the temperature and can be given by (3);

$$I_0 = I_{d0} \left(\frac{T_c}{T_{ref}} \right)^3 \exp \left[\frac{qE_g}{nk} \left(\frac{1}{T_{ref}} - \frac{1}{T_c} \right) \right] \quad (3)$$

where I_{d0} is the reverse saturation current at reference temperature T_{ref} . E_g in (4) is the bandgap energy in eV.

$$E_g = 1.16 - 7.02 \times 10^{-4} \frac{T_c^2}{T_c + 1108} \quad (4)$$

The cell temperature T_c is closely related to the solar insolation and can be estimated [44] from (5);

$$T_c = 273 + T_a + \left(\frac{NOCT - 20}{0.8} \right) G \quad (5)$$

where T_a is the ambient temperature in $^{\circ}\text{C}$, $NOCT$ is the Nominal Operating Cell Temperature, in $^{\circ}\text{C}$. From the equivalent circuit in Fig. 3, we can write the I-V relation of a PV cell as shown in (6);

$$I = I_l - I_0 \left[\exp \left(\frac{q(V + IR_s)}{nkT_c} \right) - 1 \right] - \frac{(V + IR_s)}{R_p} \quad (6)$$

where R_p is the parallel resistance. It is noted that the current I appears on both sides of Eq. (6), which implies that I cannot be expressed as an explicit function of V also I_l , I_0 and T_c are considered functions of insolation G .

III. PROPOSED KALMAN FILTER BASED MPPT TECHNIQUE

In this section, the algorithm for estimating the optimum voltage-power operating point (maximum power point) is presented. At least six voltage, \tilde{V} , and current, \tilde{I} , measurements are required in the proposed algorithm. As shown in Fig. 4, two steps are performed: curve fitting, followed by the Iterated Unscented Kalman Filter (IUKF). The advantage of the IUKF compared with the standard Kalman Filter or the Extended Kalman Filter is that it does not have a constraint on the statistical distribution of the measurement noise. The IUKF is described in details in several references [45-46]. Both steps require an initial guess for the parameters to be estimated. Six parameters are first estimated; these are the ideality factor, n , the parallel resistance, R_p , the series resistance, R_s , Cell Temperature, T_c , insolation, G , and the reverse saturation current, I_0 [47-48]. These six estimated parameters are assumed to be close to the unknown actual values of the parameters at the operation condition of the PV module. Using the estimates of these six parameters, the IUKF estimates the optimum

voltage-power output.

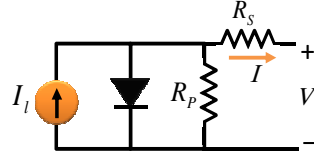


Fig. 3: PV cell single diode model [42]



Fig. 4: Proposed technique flow chart

A. Curve Fitting Method

The PV manufacturer data curves are used to estimate the six parameters. The manufacturer provides data for the variation in currents versus voltage, at constant temperature and insolation. In order to carry out the estimation, at least six measurements are needed. For each measurement, a lookup function is implemented to estimate the initial guess for the six parameters by interpolation from the manufacturer data. For each measurement, the vector of parameters' initial guesses is given by (7);

$$\hat{\chi}_{0,R/T}^k = [\hat{n}^k \quad \hat{I}_0^k \quad \hat{R}_s^k \quad \hat{R}_p^k \quad \hat{T}_c^k \quad \hat{G}^k] \quad (7)$$

where $\hat{\chi}_{0,R/T}^k$ denotes the initial guess vector, and superscript k denotes the k^{th} voltage-current measurement, and subscript 0 denotes the initial guess. The subscript R indicates that the initial guess is obtained based on constant insolation data and the subscript T denotes that the initial guess is obtained based on constant temperature data. Assume we have N measurements. There are a total of $2 \times N$ initial guess vectors. A weighted average is computed for these $2 \times N$ vectors.

First, the mean of the initial guess vectors, with respect to constant insolation and constant temperature, are calculated using (8) and (9).

$$\hat{\chi}_{0,R}^{mean} = \frac{1}{N} \sum_{k=1}^N \hat{\chi}_{0,R}^k \quad (8)$$

$$\hat{\chi}_{0,T}^{mean} = \frac{1}{N} \sum_{k=1}^N \hat{\chi}_{0,T}^k \quad (9)$$

Then, the above two means are averaged with different weights. The weight of each mean value depends on the number of changes in the domains of temperature and insolation due to the changes in the current-voltage measurements. The weights are computed using (10) and (11);

$$w_R = \frac{1}{LBR^2} + \frac{1}{UBR^2} \quad (10)$$

$$w_T = \frac{1}{LBT^2} + \frac{1}{UBT^2} \quad (11)$$

where, LBR is the number of Change of Lower boundary in Constant Insolation Data, UBR is the number of Change of

Upper boundary in Constant Insolation Data, LBT is the number of Change of Lower boundary in Constant Temperature Data, and UBT is the number of Change of Upper boundary in Constant Temperature Data. How LBR , UBR , LBT and UBT are determined is described next. Figure 5 shows five voltage-current measurements mapped into the PV array characteristic chart. Note that there are a total of five voltage-current curves for the case of constant temperature and different insolation. It is assumed that the current measured at 4V is the first measurement; the current measured at 8V is the second measurement and so on. From Figure 5, as current measurement moves from 4V to 20V, it only crosses the upper bound of the PV curve once; thus, $UBT = 1$. On the other hand, it crosses the lower bound of PV curve twice, which are at 8V to 10V and 15V to 20V. Therefore, $LBT = 2$. Similarly, both LBR and UBR can be determined using a similar approach through mapping voltage-current measurement onto PV array characteristic chart for constant irradiance case.

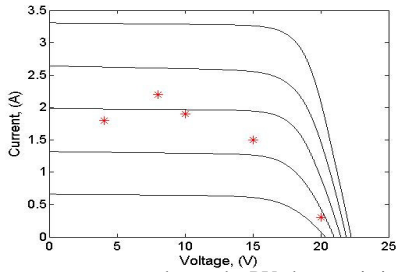


Figure 5: Measurements mapped onto the PV characteristic chart, $T = 25^{\circ}\text{C}$

The initial guess vector that will be used in the curve fitting process is given by (12).

$$\hat{x}_0 = \frac{w_R \hat{x}_{0,R}^{mean} + w_T \hat{x}_{0,T}^{mean}}{w_R + w_T} \quad (12)$$

If one or more of the LBR , UBR , LBT and UBT are equal to zeros, it results in a singularity. Therefore, further conditions to determine w_R and/or w_T will be needed. These are shown in Table 1 below.

Table 1 Additional Conditions for w_R and w_T

If $LBR = 0$ and $UBR = 0$, then $w_R = 1, w_T = 0$
If $LBT = 0$ and $UBT = 0$, then $w_R = 0, w_T = 1$
If $LBR = 0, UBR = 0, LBT = 0$ and $UBT = 0$, then $w_R = 0.5, w_T = 0.5$
If $LBR \neq 0$ and $UBR = 0$, $w_T = \frac{1}{LBT^2}$
If $LBR = 0$ and $UBR \neq 0$, $w_T = +\frac{1}{UBT^2}$
If $LBT \neq 0$ and $UBT = 0$, $w_T = \frac{1}{LBT^2}$
If $LBT = 0$ and $UBT \neq 0$, $w_T = \frac{1}{UBT^2}$

The curve fitting will estimate the six parameters such that they fit Eq. (13).

and I_{g0} is the short circuit current (3.31A for KC50T module), J_0 is the Temperature coefficient of short circuit current ($1.33 \times 10^{-3} \text{ A}/^{\circ}\text{C}$ for KC50T module), N_s is number of solar

cell in the array (36 in this case), K is the Boltzmann constant ($1.38 \times 10^{-23} \text{ J/K}$), \tilde{I}^k and \tilde{V}^k are the k^{th} current and voltage measurement set respectively. Finally, the IUKF is implemented to estimate the optimum voltage, \hat{V}_{opt} , that corresponds to the maximum power, \hat{P}_{max} , at the current condition.

$$f(\hat{x}) \equiv \tilde{I}^k - \left[\hat{I}_l - \hat{I}_0 \left(\exp \left(\frac{q(\tilde{V}^k + \tilde{I}^k \hat{R}_S)}{N_s \hat{n} \hat{T}_c K} \right) - 1 \right) - \frac{\tilde{V}^k + \tilde{I}^k \hat{R}_S}{\hat{R}_p} \right] = 0 \quad (13)$$

$$\text{where } \hat{I}_l = \frac{\hat{G}}{1000} I_{g0} + J_0 (\hat{T}_c - 298) \quad (14)$$

B. Iterated Unscented Kalman Filter

Here, the implementation of IUKF for MPP estimation is presented. For each measurement, the output power is computed. The maximum output power among all measurements is used as an initial guess for the optimal operational voltage, $\hat{V}_{opt,initial}$. In the P-V curve, the maximum power point satisfies Eq. (15).

$$\frac{dP_{max}}{dV_{opt}} = 0 \quad (15)$$

In implementing the IUKF, a pseudo measurement is employed. The pseudo measurement is the slope of the power curve. Thus, the measurement equation that corresponds to the condition in Eq. (15) is given by (16);

$$\frac{dP}{d\hat{V}_{opt}} = \hat{I}_{opt} - \left[\hat{V}_{opt} \hat{I}_0 \exp \left(\frac{q(\hat{V}_{opt} + \hat{I}_{opt} \hat{R}_S)}{N_s \hat{n} \hat{T}_c K} \right) \left[\frac{q}{N_s \hat{n} \hat{T}_c K} \right] + \frac{\hat{V}_{opt}}{\hat{R}_p} \right] \quad (16)$$

where,

$$\hat{I}_{opt} = \left[\hat{I}_l - \hat{I}_0 \left(e^{\frac{q(\hat{V}_{opt} + \hat{I}_{opt} \hat{R}_S)}{N_s \hat{n} \hat{T}_c K}} - 1 \right) - \frac{\hat{V}_{opt} + \hat{I}_{opt} \hat{R}_S}{\hat{R}_p} \right] \quad (17)$$

and \hat{I}_{opt} is the current output that corresponds to the updated \hat{V}_{opt} . The six estimated parameters ($\hat{n}, \hat{I}_0, \hat{R}_S, \hat{R}_p, \hat{T}_c, \hat{G}$), obtained from the curve fitting step, are substituted into (16) and (17) to estimate both \hat{V}_{opt} and \hat{I}_{opt} . The IUKF process is as follows. First, the initial guess is obtained for $\hat{V}_{opt,initial}$ using (15). Then the state covariance, $\hat{\rho}$, which is also known as the level of confidence or the expected error boundary of the estimated parameters, is initialized. Next, a sigma point (σ) is generated using the state covariance, and \hat{V}_{opt} is mapped into the sigma point [49] as shown by (18);

$$\vec{\hat{V}}_{opt} = [\hat{V}_{opt} \quad \hat{V}_{opt} + \sigma \quad \hat{V}_{opt} - \sigma]^T \quad (18)$$

with

$$\sigma = \sqrt{(L + \lambda)(\bar{\rho} + Q)} \quad (19)$$

where, Q is the process noise variance, L is the number of estimated states, which is one in this case, and λ is given (20);

$$\lambda = \alpha^2(L + \kappa) - L \quad (20)$$

where the α is a constant small positive value, ($1 \times 10^{-4} \leq \alpha \leq 1$) [45], that determine the spread of sigma point around the estimated states. The κ is usually given by (21) as in [40].

$$\kappa = 3 - L \quad (21)$$

Then, for each of the mapped states in \vec{V}_{opt} in (18), the corresponding estimated optimum current, \vec{I}_{opt} , for each mapped \vec{V}_{opt} is calculated based on (6). For each set of estimated \vec{V}_{opt} and \vec{I}_{opt} , an estimated pseudo measurement is calculated using (16). Let the estimated pseudo measurement vector be that in (22);

$$\hat{\gamma} = [\hat{\gamma}_1 \quad \hat{\gamma}_2 \quad \hat{\gamma}_3]^T \quad (22)$$

where $\hat{\gamma}_1$ is evaluated at (\vec{V}_{opt}) , $\hat{\gamma}_2$ is evaluated at $(\vec{V}_{opt} + \sigma)$, and $\hat{\gamma}_3$ is evaluated at $(\vec{V}_{opt} - \sigma)$. As mentioned in section III, the advantage of the IUKF when compared with the standard Kalman Filter or the Extended Kalman Filter is that it does not have a constraint on the statistical distribution of the measurement noise. This is critical in this problem, since (16) shows that the estimation errors exhibits non-Gaussian noise. The mean by which the Unscented update gain is determined is described next. First, four weight variables are given as in (23)-(26);

$$W_0^{mean} = \frac{\lambda}{L + \lambda} \quad (23)$$

$$W_0^{cov} = \frac{\lambda}{L + \lambda} + (1 - \alpha^2 + \beta) \quad (24)$$

$$W_i^{mean} = W_i^{cov} = \frac{1}{2(L + \lambda)} \quad (25)$$

$$W_i^{cov} = W_i^{mean} \quad (26)$$

where, β is an arbitrary constant. A good initial guess for β is 2 [40]. Next, the mean of the mappings of the estimated optimum voltage, and the estimated measurements are calculated as using (27) and (28).

$$\hat{V}_{opt}^{mean} = \sum_{i=0}^{2L} W_i^{mean} \vec{V}_{opt}(i + 1) \quad (27)$$

$$\hat{\gamma}^{mean} = \sum_{i=0}^{2L} W_i^{mean} \hat{\gamma}(i + 1) \quad (28)$$

At $i = 0$, W_i^{mean} is calculated using (23), when $i \neq 0$, W_i^{mean} is calculated using (25). Next, the predicted covariance of the mappings of the estimated optimum voltage and the

pseudo measurements are found using (29)-(31) [49].

$$\begin{aligned} \wp^{xx} = & \sum_{i=0}^{2L} W_i^{cov} \left[\vec{V}_{opt}(i + 1) \right. \\ & \left. - \hat{V}_{opt}^{mean} \right] \left[\vec{V}_{opt}(i + 1) - \hat{V}_{opt}^{mean} \right]^T \end{aligned} \quad (29)$$

$$\begin{aligned} \wp^{yy} = & \sum_{i=0}^{2L} W_i^{cov} \left[\hat{\gamma}(i + 1) \right. \\ & \left. - \hat{\gamma}^{mean} \right] \left[\hat{\gamma}(i + 1) - \hat{\gamma}^{mean} \right]^T \end{aligned} \quad (30)$$

$$\begin{aligned} \wp^{xy} = & \sum_{i=0}^{2L} W_i^{cov} \left[\vec{V}_{opt}(i + 1) \right. \\ & \left. - \hat{V}_{opt}^{mean} \right] \left[\hat{\gamma}(i + 1) - \hat{\gamma}^{mean} \right]^T \end{aligned} \quad (31)$$

Finally, the estimated optimum voltage and its covariance are updated using (32) and (33);

$$\hat{V}_{opt} = \hat{V}_{opt} - \wp^{xy} (\wp^{yy} + \mathfrak{R})^{-1} \hat{\gamma}^{mean} \quad (32)$$

$$\bar{\rho} = \bar{\rho} - \wp^{xy} (\wp^{yy} + \mathfrak{R})^{-T} (\wp^{xy})^T \quad (33)$$

where \mathfrak{R} is the pseudo measurement noise covariance. A small value of \mathfrak{R} is assumed to avoid singularity in $(\wp^{yy} + \mathfrak{R})^{-1}$. The optimum current, \hat{I}_{opt} , that corresponds to the updated \hat{V}_{opt} is recalculated using (17). The iteration process is repeated until it meets the designated maximum iteration, or until the error between the estimated pseudo measurement and the desired measurement falls within a threshold set by (34).

$$abs(0 - \hat{\gamma}^{mean}) \leq 10^{-6} \quad (34)$$

IV. SIMULATION RESULTS

Assume the simulation environment of the PV module to be at 600 W/m² solar insolation, and a cell temperature is 25°C. To study the impact of the collected measurements on the accuracy of estimation in the proposed technique, six sets (each has six measurements) are assumed. The six measurement sets are given by (35)-(46).

$$\vec{I}_1 = [1.96 \quad 1.95 \quad 1.94 \quad 1.92 \quad 1.90 \quad 1.86]^T A \quad (35)$$

$$\vec{V}_1 = [0 \quad 5.4 \quad 10 \quad 15 \quad 16.4 \quad 17]^T V \quad (36)$$

$$\vec{I}_2 = [1.96 \quad 1.95 \quad 1.94 \quad 1.74 \quad 1.39 \quad 0.91]^T A \quad (37)$$

$$\vec{V}_2 = [0 \quad 5.4 \quad 10 \quad 17.8 \quad 19 \quad 20]^T V \quad (38)$$

$$\vec{I}_3 = [1.96 \quad 1.95 \quad 1.94 \quad 0.8 \quad 0.31 \quad 0]^T A \quad (39)$$

$$\vec{V}_3 = [0 \quad 5.4 \quad 10 \quad 20.2 \quad 21 \quad 21.5]^T V \quad (40)$$

$$\vec{I}_4 = [1.74 \quad 1.39 \quad 0.91 \quad 1.92 \quad 1.90 \quad 1.86]^T A \quad (41)$$

$$\vec{V}_4 = [17.8 \quad 19 \quad 20 \quad 15 \quad 16.4 \quad 17]^T V \quad (42)$$

$$\vec{I}_5 = [1.74 \quad 1.39 \quad 0.91 \quad 0.8 \quad 0.31 \quad 0]^T A \quad (43)$$

$$\vec{V}_5 = [17.8 \quad 19 \quad 20 \quad 20.2 \quad 21 \quad 21.5]^T V \quad (44)$$

$$\hat{I}_6 = [1.92 \ 1.90 \ 1.86 \ 0.8 \ 0.31 \ 0]^T A \quad (45)$$

$$\hat{V}_6 = [15 \ 16.4 \ 17 \ 20.2 \ 21 \ 21.5]^T V \quad (46)$$

Each measurement set is used in the curve fitting step presented in Section III-A to estimate the six parameters, n , R_p , R_s , T_c , G , and I_0 . Then, each set of the six parameters is used in the IUKF to estimate the MPP for each given measurement set. The initial estimated state covariance for each measurement set is $\hat{\sigma} = 25$. The pseudo measurement noise covariance is $\mathfrak{R} = 10^{-4}$, the process noise variance is $Q = 10^{-16} V^2$, and the maximum number of iterations for the IUKF process is 10000. Figures 6 and 7 show the I-V and P-V plots for the six sets of measurements. It is desired to have small variations in the output power while collecting the six measurements necessary for estimation. Fig. 6 shows that the power fluctuation is between 0-40W for the six measurement sets. Measurement sets 3 and 4 have the lowest power fluctuations among them.

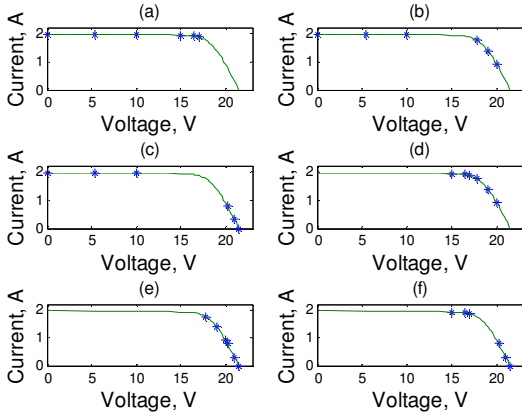


Fig. 6: I-V plots for measurement sets 1 (a) to 6 (f), respectively.

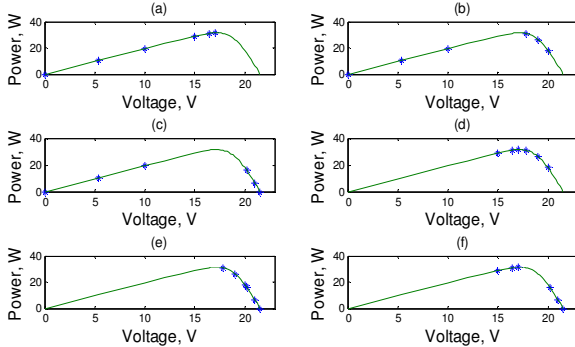


Fig. 7: P-V plots for measurement sets 1 (a) to 6 (f), respectively.

Simulation results are listed in Table 2. Table 2 shows comparisons between the estimated optimum voltages, maximum power outputs, cell temperatures and solar irradiances for the six sets of measurements. The results from Table 2 show that, in general, better estimates are obtained when the measurement points cover the majority of the I-V curve. In all cases, the error in the estimated optimal voltage is less than 3%. Both the cell temperature, T_c , and the solar insolation, G , shown in Table 2 are estimated using the curve fitting approach. In addition,

Table 3 compares the other four estimated parameters using the curve fitting method. Because the four parameters vary with respect to both cell temperature and solar insolation, the true value of each parameter is unknown. Table 3 shows that the variance of the estimated ideality factor and estimated series and parallel resistor, is around 10%. However, due to the fact that the reverse saturation current is very small, the variance of \hat{I}_0 among measurements is relatively large.

Table 2 Comparison between estimation results and actual values.

No. of Measurement Sets	V_{opt}, V	P_{max}, W	T_c, K	$G, W/m^2$
1	17.35	32.27	291	597
2	17.04	31.59	298	595
3	16.75	30.63	300	594
4	17.01	31.26	312	576
5	16.53	32.62	303	639
6	16.77	31.55	298	604
TRUE	17.00	31.54	298	600

Table 3 Estimated parameters using curve fitting

No. of Measurement Sets	\hat{n}	\hat{I}_0, A	\hat{R}_s, Ω	\hat{R}_p, Ω
1	1.15	3.05×10^{-9}	0.898	594.22
2	1.08	1.00×10^{-9}	0.739	602.99
3	1.21	8.06×10^{-9}	0.878	544.31
4	1.12	1.00×10^{-9}	0.633	575.68
5	1.21	6.84×10^{-9}	0.924	616.15
6	1.09	1.00×10^{-9}	0.966	583.50

Fig. 8 shows that all the estimated optimum-power voltages are close to the true maximum power voltage. In reality, all operating points lie on the true power-voltage curve, however, due to error in the estimated parameters, the estimated power is off the true curve by a few points. The error in the estimated optimal voltage is limited to 3%. When carrying out the experiment in reality, the output power at any of the estimated optimum voltage points will be on the true P-V curve. So, we can define the modified estimated optimal power (MEOP) at each point as the power at the estimated optimal voltage as read from the true P-V curve. As can be seen from Fig. 7, the error between the MEOP and the true optimal power point is less than 0.5W.

V. EXPERIMENTAL RESULTS

In order to validate the proposed technique's effectiveness, a practical setup is arranged. Fig. 9 shows details of the experimental setup. A 32-bit, 150 MHz digital signal controller TMS320F28335 is used as the main controller. The power circuit is basically a boost converter with parameters listed in Table 4. In order to show that the proposed Kalman filter based MPPT can achieve satisfactory practical results at different environmental conditions, the PV array in the previously described experimental rig is forced by the boost converter controller to run at six different points on its P-V curve. When

the steady state is reached at each point, the corresponding array voltage, array current and array power are stored.

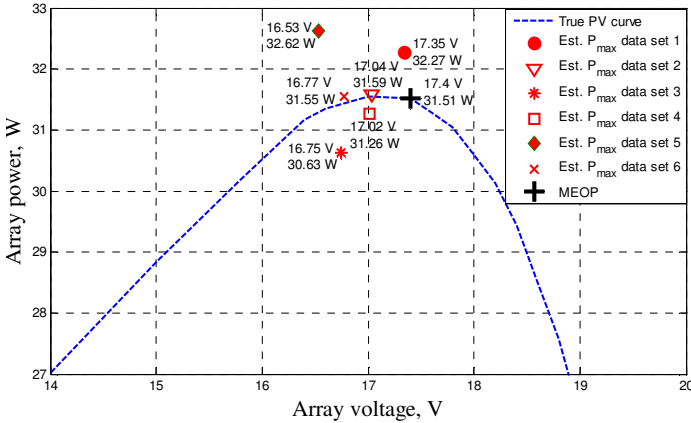


Fig.8: True P-V curve and the six estimated V_{opt} - P_{max} points.

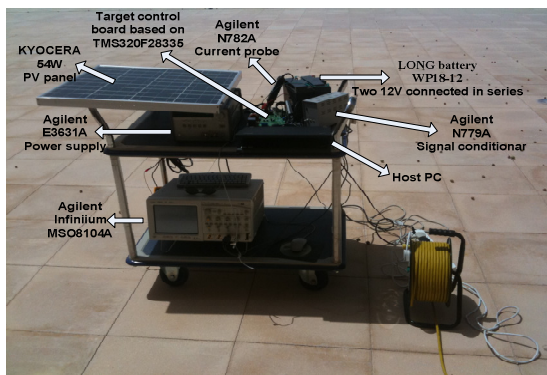


Fig. 9: Experimental test rig, Texas A&M university at Qatar outdoor atrium

Table 4: Experimental setup components list

Element	Manufacturer and part number	Value
Inductor	Coilcraft	402 μ H, 3.7A
	DMT3-402-3.7L	Toroidal power choke
Capacitor	-	3x1200 μ F, 35V electrolytic capacitors
	ON semiconductors	50V, 4A ultrafast recovery diode
Diode	MUR405	
IGBT	International Rectifiers	600V, 6.5A
	IRG4BC20UD	IGBT with ultrafast recovery diode
Load	LONG battery	2x12V
	WP18-12	connected in series
PV array	KYOCERA	54W
	KC50T	Solar panel

Then, applying the proposed Kalman filter based MPPT technique yields the optimum operating voltage that corresponds to the maximum array power. After that, the boost converter controller forces the PV array to run at this optimum operating array voltage. These previously mentioned steps are repeated at different time intervals (creating five sets, from Set 1 to Set 5) all over the day to achieve testing of the proposed Kalman filter based MPPT at different insolation and temperature conditions. Fig. 10 shows the block diagram of the experimental setup while

the software flow chart is shown in Fig. 11. Fig. 12 shows the experimental results of the proposed Kalman filter based MPPT for various environmental conditions. It can be shown that the proposed technique is capable of approaching an operating point very close to the optimum operating point that corresponds to the maximum power. A slight deviation occurs, although minimal, in the experimental results, mainly because of the measurement error and the fact that while the six measurement points are taken, the sun movement creates varying insolation levels and temperature variation during the measurements which are not compensated in the proposed technique. Moreover, despite the errors due to PV parameter estimation, the experimental results show promising performance and accurate tracking.

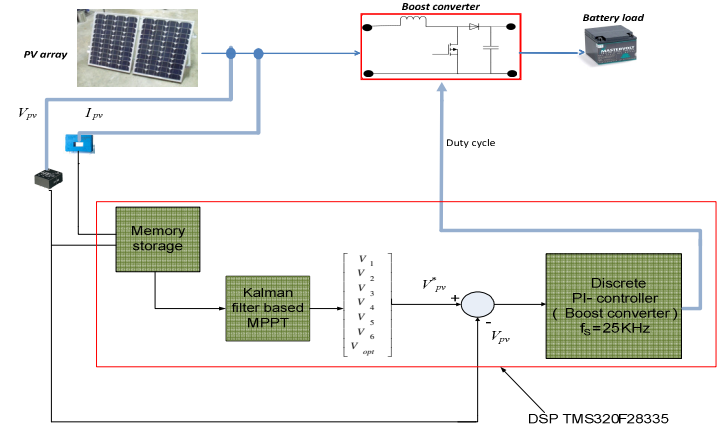


Fig. 10: Experimental setup block diagram

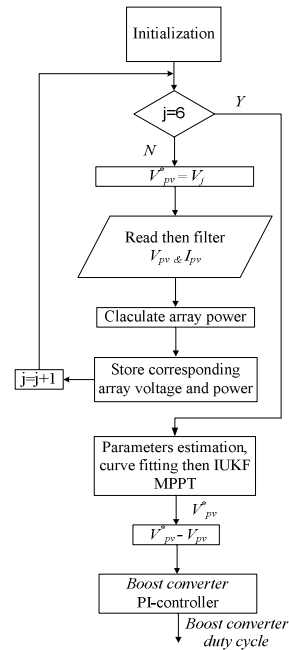


Fig. 11. software flow chart

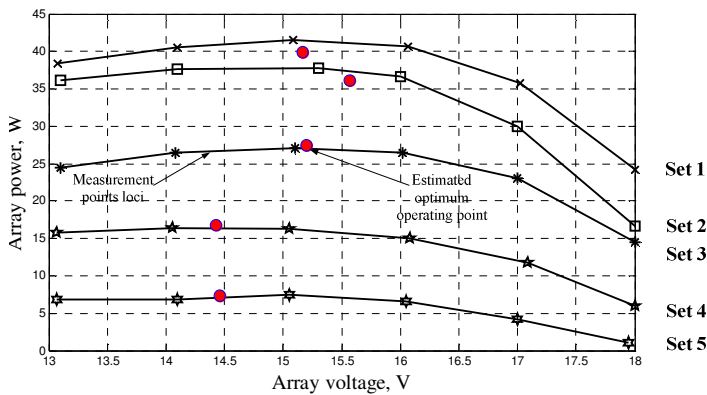


Fig. 12: Experimental results P-V curves

VI. CONCLUSION

In this paper, an Iterated Unscented Kalman Filter based MPPT technique for PV applications has been presented. The proposed technique is generic, adaptive and does not require neither pre-set constants, like other P&O techniques, nor curve scanning, like other hill climbing techniques. Only six operating points on the PV curve are required as inputs to the proposed technique. The proposed method in this paper can be applied on any PV system using the corresponding PV array data sheet. The filter derivation and governing equations have been illustrated in detail. Simulation results for various operating points have been carried out. An experimental setup has been developed with practical results at various irradiance conditions to validate the proposed technique's effectiveness.

ACKNOWLEDGEMENT

This publication was made possible by NPRP grant (NPRP 4-941-2-356) from the Qatar National Research Fund (a member of Qatar Foundation).

REFERENCES

- [1] Online: http://re.jrc.ec.europa.eu/esti/index_en.htm, accessed March 2012
- [2] Liserre, M.; Sauter, T.; Hung, J.Y.; , "Future Energy Systems: Integrating Renewable Energy Sources into the Smart Power Grid Through Industrial Electronics," *Industrial Electronics Magazine, IEEE* , vol.4, no.1, pp.18-37, March 2010
- [3] Esram, T.; Chapman, P.L.; , "Comparison of Photovoltaic Array Maximum Power Point Tracking Techniques," *Energy Conversion, IEEE Transactions on* , vol.22, no.2, pp.439-449, June 2007
- [4] O. Hashimoto, T. Shimizu, and G. Kimura, "A novel high performance utility interactive photovoltaic inverter system," in *Conf. Record 2000 IEEE Ind. Applicat. Conf.*, 2000, pp. 2255–2260.
- [5] E. Koutroulis, K. Kalaitzakis, and N. C. Voulgaris, "Development of a microcontroller-based, photovoltaic maximum power point tracking control system," *IEEE Trans. Power Electron.*, vol. 16, no. 21, pp. 46–54, Jan. 2001.
- [6] M.Veerachary, T. Senjyu, and K.Uezato, "Maximum power point tracking control of IDB converter supplied PV system," in *IEE Proc. Elect. Power Applicat.*, 2001, pp. 494–502.

- [7] W. Xiao and W. G. Dunford, "A modified adaptive hill climbing MPPT method for photovoltaic power systems," in *Proc. 35th Annu. IEEE Power Electron. Spec. Conf.*, 2004, pp. 1957–1963.
- [8] N. Femia, G. Petrone, G. Spagnuolo, and M. Vitelli, "Optimization of perturb and observe maximum power point tracking method," *IEEE Trans. Power Electron.*, vol. 20, no. 4, pp. 963–973, Jul. 2005.
- [9] N. Kasa, T. Iida, and L. Chen, "Flyback inverter controlled by sensorless current MPPT for photovoltaic power system," *IEEE Trans. Ind. Electron.*, vol. 52, no. 4, pp. 1145–1152, Aug. 2005.
- [10] S. Jain and V. Agarwal, "A new algorithm for rapid tracking of approximate maximum power point in photovoltaic systems," *IEEE Power Electron. Lett.*, vol. 2, no. 1, pp. 16–19, Mar. 2004.
- [11] T. Tafticht and K. Agbossou, "Development of a MPPT method for photovoltaic systems," in *Canadian Conf. Elect. Comput. Eng.*, 2004, pp. 1123–1126.
- [12] K. Irisawa, T. Saito, I. Takano, and Y. Sawada, "Maximum power point tracking control of photovoltaic generation system under non-uniform insolation by means of monitoring cells," in *Conf. Record Twenty-Eighth IEEE Photovoltaic Spec. Conf.*, 2000, pp. 1707–1710.
- [13] T.-Y. Kim, H.-G. Ahn, S. K. Park, and Y.-K. Lee, "A novel maximum power point tracking control for photovoltaic power system under rapidly changing solar radiation," in *IEEE Int. Symp. Ind. Electron.*, 2001, pp. 1011–1014.
- [14] Y.-C. Kuo, T.-J. Liang, and J.-F. Chen, "Novel maximum-power-point tracking controller for photovoltaic energy conversion system," *IEEE Trans. Ind. Electron.*, vol. 48, no. 3, pp. 594–601, Jun. 2001.
- [15] K. Kobayashi, I. Takano, and Y. Sawada, "A study on a two stage maximum power point tracking control of a photovoltaic system under partially shaded insolation conditions," in *IEEE Power Eng. Soc. Gen. Meet.*, 2003, pp. 2612–2617.
- [16] G. W. Hart, H. M. Branz, and C. H. Cox, "Experimental tests of open loop maximum-power-point tracking techniques," *Solar Cells*, vol. 13, pp. 185–195, 1984.
- [17] M. A. S. Masoum, H. Dehbonei, and E. F. Fuchs, "Theoretical and experimental analyses of photovoltaic systems with voltage and current-based maximum power-point tracking," *IEEE Trans. Energy Convers.*, vol. 17, no. 4, pp. 514–522, Dec. 2002.
- [18] H.-J. Noh, D.-Y. Lee, and D.-S. Hyun, "An improved MPPT converter with current compensation method for small scaled PV-applications," in *Proc. 28th Annu. Conf. Ind. Electron. Soc.*, 2002, pp. 1113–1118.
- [19] T. Noguchi, S. Togashi, and R. Nakamoto, "Short-current pulse based adaptive maximum-power-point tracking for photovoltaic power generation system," in *Proc. 2000 IEEE Int. Symp. Ind. Electron.*, 2000, pp. 157–162.
- [20] A. M. A. Mahmoud, H. M. Mashaly, S. A. Kandil, H. El Khashab, and M. N. F. Nashed, "Fuzzy logic implementation for photovoltaic maximum power tracking," in *Proc. 9th IEEE Int. Workshop Robot Human Interactive Comm.*, 2000, pp. 155–160.
- [21] Patcharaprakiti, N.; Premrudeepreechacharn, S.; , "Maximum power point tracking using adaptive fuzzy logic control for grid-connected photovoltaic system," *Power Engineering Society Winter Meeting, 2002. IEEE* , vol.1, no., pp. 372-377 vol.1, 2002
- [22] T. Hiyama, S. Kouzuma, and T. Imakubo, "Identification of optimal operating point of PV modules using neural network for real time maximum power tracking control," *IEEE Trans. Energy Convers.*, vol. 10, no. 2, pp. 360–367, Jun. 1995.

- [23] K. Ro and S. Rahman, "Two-loop controller for maximizing performance of a grid-connected photovoltaic-fuel cell hybrid power plant," *IEEE Trans. Energy Convers.*, vol. 13, no. 3, pp. 276–281, Sep. 1998.
- [24] L. Zhang, Y. Bai, and A. Al-Amoudi, "GA-RBF neural network based maximum power point tracking for grid-connected photovoltaic systems," in *Proc. Int.Conf. Power Electron. Machines and Drives*, 2002, pp. 18–23.
- [25] Salvatore, N.; Caponio, A.; Neri, F.; Stasi, S.; Cascella, G.L.; , "Optimization of Delayed-State Kalman-Filter-Based Algorithm via Differential Evolution for Sensorless Control of Induction Motors," *Industrial Electronics*, *IEEE Transactions on* , vol.57, no.1, pp.385-394, Jan. 2010
- [26] Barut, M.; Bogosyan, S.; Gokasan, M.; , "Experimental Evaluation of Braided EKF for Sensorless Control of Induction Motors," *Industrial Electronics*, *IEEE Transactions on* , vol.55, no.2, pp.620-632, Feb. 2008
- [27] de Santana, E.S.; Bim, E.; do Amaral, W.C.; , "A Predictive Algorithm for Controlling Speed and Rotor Flux of Induction Motor," *Industrial Electronics*, *IEEE Transactions on* , vol.55, no.12, pp.4398-4407, Dec. 2008
- [28] Szabat, K.; Orłowska-Kowalska, T.; , "Performance Improvement of Industrial Drives With Mechanical Elasticity Using Nonlinear Adaptive Kalman Filter," *Industrial Electronics*, *IEEE Transactions on* , vol.55, no.3, pp.1075-1084, March 2008
- [29] Agha Zadeh, R.; Ghosh, A.; Ledwich, G.; , "Combination of Kalman Filter and Least-Error Square Techniques in Power System," *Power Delivery*, *IEEE Transactions on* , vol.25, no.4, pp.2868-2880, Oct. 2010
- [30] Chen, C.I.; Chang, G.W.; Hong, R.C.; Li, H.M.; , "Extended Real Model of Kalman Filter for Time-Varying Harmonics Estimation," *Power Delivery*, *IEEE Transactions on* , vol.25, no.1, pp.17-26, Jan. 2010
- [31] Won, S.-h.P.; Melek, W.W.; Golnaraghi, F.; , "A Kalman/Particle Filter-Based Position and Orientation Estimation Method Using a Position Sensor/Inertial Measurement Unit Hybrid System," *Industrial Electronics*, *IEEE Transactions on* , vol.57, no.5, pp.1787-1798, May 2010
- [32] Won, S.-h.P.; Golnaraghi, F.; Melek, W.W.; , "A Fastening Tool Tracking System Using an IMU and a Position Sensor With Kalman Filters and a Fuzzy Expert System," *Industrial Electronics*, *IEEE Transactions on* , vol.56, no.5, pp.1782-1792, May 2009
- [33] Mitsantisuk, C.; Katsura, S.; Ohishi, K.; , "Kalman-Filter-Based Sensor Integration of Variable Power Assist Control Based on Human Stiffness Estimation," *Industrial Electronics*, *IEEE Transactions on* , vol.56, no.10, pp.3897-3905, Oct. 2009
- [34] Pinjia Zhang; Yi Du; Jing Dai; Habetler, T.G.; Bin Lu; , "Impaired-Cooling-Condition Detection Using DC Signal Injection for Soft-Starter-Connected Induction Motors," *Industrial Electronics*, *IEEE Transactions on* , vol.56, no.11, pp.4642-4650, Nov. 2009
- [35] Beccuti, A.G.; Mariethoz, S.; Cliquennois, S.; Shu Wang; Morari, M.; , "Explicit Model Predictive Control of DC–DC Switched-Mode Power Supplies With Extended Kalman Filtering," *Industrial Electronics*, *IEEE Transactions on* , vol.56, no.6, pp.1864-1874, June 2009
- [36] Liserre, M.; Pigazo, A.; Dell'Aquila, A.; Moreno, V.M.; , "An Anti-Islanding Method for Single- Phase Inverters Based on a Grid Voltage Sensorless Control," *Industrial Electronics*, *IEEE Transactions on* , vol.53, no.5, pp.1418-1426, Oct. 2006
- [37] Y. Bar-Shalom, X. Li and T. Kirubarajan, "Estimation with applications to Tracking and Navigation, Theory Algorithms and Software," John Wiley & Sons, 2001.
- [38] R. Kalman, "A New Approach to Linear Filtering and Prediction Problems," *Transactions of the ASME - Journal of Basic Engineering*, 82 (Series D), 1960 pp. 35-45
- [39] D. Simon, "Optimal State Estimation, Kalman, H ∞ and Nonlinear Approaches," John Wiley and Sons, 2006.
- [40] J. Crassidis, and J. Junkins, "Optimal Estimation of Dynamic Systems," Chapman & Hall/CRC, 2004.
- [41] Online: <http://www.kyocerasolar.com/pdf/specsheets/KC50T.pdf>; accessed March 2012
- [42] Mrakvart T.: 'Solar electricity' (Wiley, New York, 2000, 2nd edn.)
- [43] Gow J.A., Manning C.D.: 'Development of a photovoltaic array model for use in power electronics simulation studies', *IEE Proc. EPA*, 1999, 146, (2), pp. 193–200
- [44] Messenge R., Ventre J.: 'Photovoltaic systems engineering' (CRC Press, Boca Raton, FL, 2004, 2nd edn.), p. 54
- [45] Banani, S.A. and Masnadi-Shirazi, M.A., "A New Version of Unscented Kalman Filter." *World Academy of Science, Engineering and Technology*, vol. 26, pp 192-197.
- [46] Sibley, Gabe, Sukhatme, Gaurav and Matthies, Larry., "The Iterated Sigma Point Kalman Filter with Applications to Long Range Stereo." Philadelphia : *Proceedings of Robotics: Science and Systems*, 2006.
- [47] Karatepe, Engin, Boztepe, Mutlu and Colak, Metin., "Development of a suitable model for characterizing photovoltaic arrays with shaded solar cells." *s.l. : Solar Energy* 81 , 2006.
- [48] Wang, Y.-J and Hsu, P.-C., "Analytical modelling of partial shading and different orientation of photovoltaic modules." *s.l. : Renewable Power Generation, IET*, 2010, Issue 3, Vol. 4.
- [49] Julier, S.J., Uhlmann, J.K. and Durrant-Whyte, H.F., "A New Method for the Nonlinear Transformation of Means and Covariances in Filters and Estimators." *s.l. : IEEE Transactions on Automatic Control*, March 2000, Vols. AC-45, pp. 477-482. 3.